Manuscript

Click here to view linked References

Chem

For more detailed guidelines on formatting your paper, please see our Information for Authors.

CellPress

Article

Photo-assembling cyclic peptides for dynamic light-driven peptide nanotubes

Marcos Vilela-Picos,[1] Federica Novelli,[1] Antía Pazó,[1] Alejandro Méndez-Ardoy,[1] Giulia Marafon,[2] Manuel Amorín,[1] Alessandro Moretto,[2] Juan R. Granja[1,*]

[1] Centro Singular de Investigación en Química Biolóxica e Materiais Moleculares (CiQUS), Departamento de Química Orgánica, Universidade de Santiago de Compostela, 15782 Santiago de Compostela, Spain

[2] Department of Chemical Sciences, University of Padova, via Marzolo, 1, Padova (Italy)

*Correspondence: juanr.granja@usc.es

SUMMARY

Cyclic peptides containing a β-unsaturated amino acid are programmed to switch between monomeric form and self-assembled peptide nanotube structures upon light irradiation. The process is triggered by the reversible *E*-Z isomerization of the unsaturated β-amino acid that forces the peptide to swap from the folded (unassembled) to the flat conformation (assembled). The process is also tuned by the pH media, which provides a double check-point control in the molecular assembly of the peptide nanotubes. The light-driven assembly process can be triggered in confined environment and the resulting nanotubes allow the inter-vesicles communication providing droplets with self-fusiogenic properties.

Self-assembly, photoassembler, photoswitching, cyclic peptides, nanotubes, fusiogenic

INTRODUCTION

Photoassemblers are molecular units whose assembly properties are modulated by light-induced conformational changes.[1,2] Among others, azobenzene moieties represent one of the most powerful tools because of the significant structural changes between the two isomers (*E* or *Z*).[3] Photo-switchable peptides have emerged as useful materials for various applications ranging from new drugs to reversible components for supramolecular biomaterials.[4,5] Most of these materials are related to changes in the secondary structure derived from the light-induced isomerization of a photoswitchable component. Recently, some of us synthesized unsaturated β-alanine derivative (3-aminoprop-2-enoic acid) to prepare peptide-based conformational switchers through the *E* to *Z*–isomerization of this derivative.[6,7,8] While the *cis*-isomer adopts a loop-like structure, the extended conformation (*trans*-isomer) allows the generation of ribbons through the formation of β-sheet type structures.

Self-assembling cyclic peptide nanotubes (SCPNs) are tubular-shaped structures formed by the controlled stacking of cyclic peptide (CP) components that adopt a planar-shaped conformation.[9,10] The resulting hollow 1D materials have two different surfaces (inner and outer faces), making them very powerful nanobiomaterials.[10] These supramolecular polymers are constructed by establishing hydrogen-bonding interactions between adjacent peptide backbones. The cooperative enthalpic contribution of each hydrogen-bonding interaction is the driving force that impels the nanotube formation. In the last years, we and others have been able to tune the spatiotemporal control of SCPNs formation.[11,12] Although the strong cooperativity in nanotube formation allows triggering the assembly under specific mild conditions, unfortunately, the reverse process (nanotube dissociation) is not so simple, usually requiring slightly more severe conditions. The use of polymeric chains attached to cyclic peptides, which reduce the dynamism of the molecular assembly,[13] allowed the implementation of milder conditions, but further studies are still needed to make this reversibility available for all types of SCPNs.[14] In addition, fast and precise spatiotemporal

resolution to external stimuli is also pursued, especially in confined spaces such as living cells. Here, we present a novel kind of *D,L*-α-cyclic peptide nanotubes that incorporate a β-unsaturated photosensitive amino acid whose assembly/disassembly can be induced light.[15,16] The nanotube formation can be produced in confined spaces and the resulting vesicles showed fusiogenic properties forcing the water-in-oil droplets fusion under neutral conditions.[17]

Very recently, we have shown that the incorporation of β-residues on an alternating *D,L*-cyclic peptide (*D,L*-α-CP), the main kind of SCPNs,[9,10] did not prevent the nanotube formation, although restricts its stacking exclusively to parallel-type β-sheet structures.[18] Pristine *D,L*-α-CPs can be stacked to form parallel or antiparallel structures because the NH and carbonyl of each residue are oriented in the same direction, providing planar conformations that have the same number of hydrogen bond donors and acceptors on each side of the cycle.[19,20] However, the β-residues in the extended conformation arrange these groups pointing in opposite directions and, consequently, can only form parallel β-sheets-based SCPNs.[21] Therefore, because of the uneven distribution of the hydrogen bonding donors and acceptors at both faces of the flat ring-shaped structure, the hybrid peptides, as the one described here, can only stack in a parallel fashion.

RESULTS AND DISCUSSION

Design and synthesis of cyclic peptides

In this work, we introduced the 3-aminoprop-2-enoic acid (ΔβAla),[7] a residue that can exist as either *Z*- or *E*-isomers (Δ^{Z}βAla or Δ^{E}βAla, respectively), in nanotube forming CPs. Both forms can be interconverted by appropriate UV light-irradiation. The shorter wavelength (254 nm) is used to transform the *trans*-derivative to the *cis*-isomer, while irradiation with a longer wavelength light (290-320 nm) provides the thermodynamically more stable *E*-isomer. We intend to use this process to change the conformational shape of the CPs from a folded conformation (monomeric component) to the flat ring-shaped conformation that is programmed to self-assemble and *vice versa*. Based on previous work in which the incorporation of one or two β-alanine to *D,L*-α-CPs provided a new kind of SCPNs constituted by parallel oriented stacks,[18] now we decided to replace one of the β-Ala by the corresponding unsaturated residue. Therefore, cyclic peptide **^{E}CP1** (Fig. 1A) was designed based on the previously established designs. This peptide was prepared using Fmoc-methodologies on solid phase synthesis using a Rink amide resin.[22,23] For this purpose, the Glu residue was attached through its side chain using an α-allyl-protected glutamic acid derivative (**1**). The olefinic moiety of the unsaturated residue was masked as a furan cycloadduct of Fmoc-Δ^{Z}βAla-OH (**2**).[6] Cycloadduct **2** was attached, as a racemic mixture, at the end of the peptide sequence. After this, the cyclization was carried out on solid support. To this end, the C-terminal allyl-protecting group was removed using typical π-allyl palladium chemistry, and then the N-terminal Fmoc group was eliminated using standard conditions (25% piperidine in DMF). The cyclization was carried out using PyAOP as a coupling regent. The reaction was followed by HPLC analysis of acidic cocktails resulting from cleavage of small portions of resin (2-3 mg). Full cyclization was achieved after 2 h of reaction time and then the pyrene moiety was incorporated on the Lys side chain by treatment with mild acidic conditions [HFIP/TFE/TIS/DCM (20:10:5:65)] followed by coupling of 1-pyreneacetic (**3**) using *N*-HATU as coupling agent.[12] Peptide cleavage was carried out using standard conditions [TFA/DCM/H_2O/TIS (90:5:2.5:2.5)]. Under these conditions, the resulting major product had a molecular weight two units higher than the expected. This compound was assigned to the cyclic peptide with the double bond of the cycloadduct moiety reduced. We attributed this problem to the strong reducing properties of the silane scavenger. Therefore, substitution of this reagent by thioanisole (MPS) [TFA/DCM/H_2O/MPS (90:5:2.5:2.5)] provided, after HPLC purification, **CP2** in an overall 18% yield. Heating an aqueous solution (H_2O/ACN, 1:1) of this peptide for 24h at 80 ºC yielded the expected **^{Z}CP1** (Fig. 1A). The chemical shift of amide proton of Δ^{Z}βAla at 11.28 ppm supports the proposed folded conformation of **^{Z}CP1**, consistent with the previously reported behavior of peptides containing this residue due to the formation of a strong hydrogen bond with its carbonyl moiety.[7] The sharp and fine resolution of most of the proton signals of this CP confirms that it is unaggregated (Fig. S1).

Studies of cyclic peptide isomerization

The *E*-isomer was obtained by irradiation (290-320 nm) of an aqueous solution of **^{Z}CP1** (400 μM) for 10 min (Fig. 1A). Under this conditions **^{E}CP1** was obtained as major product, in a 7 to 3 mixture with the starting peptide. Both isomers were separated by HPLC, and the new compound was characterized. The NMR signals at acidic conditions (pH<3.5, Fig. S2) confirm the up-field shift (9.79 ppm) of the amide proton of Δ^{E}BAla, suggesting that it is not anymore participating in the above-mentioned strong intramolecular hydrogen bond. The FTIR spectrum (Fig. S3) of a lyophilized sample after neutralization supports the formation of a parallel-*like* β-sheet structure with a strong band at 1633 cm^{-1} and a shoulder at 1659 cm^{-1}.[18] In addition, the band at 3293 cm^{-1} (amide A) is highly indicative of a well-established network of hydrogen bonds.[24]

The kinetic of this conversion was followed by HPLC (200 μM, Fig. 1B and 1C). After 10 min of irradiation, the mixture already reaches the steady state as a 7:3 mixture of both isomers. This ratio is slightly smaller than the previously reported studies, suggesting that the internal hydrogen bond in the CP must stabilize the Z-isomer.[7] The isomerization is independent of the pH of the media, as confirmed by the similar ratios and yields obtained at either acidic (pH 1.8), native (pH 5.1), neutral (pH 7.0) or basic conditions (pH 9.0), see Fig. S4. Under neutral and basic conditions, the peptide starts to precipitate during irradiation due, most likely, to pH-induced self-assembly, as denoted by the reduction of the sample signals with time.

The isomerization of **^{E}CP1** (200 μM, Fig. 1D and 1E) into **^{Z}CP1** was also investigated but using a shorter wavelength (254 nm). The reaction was also studied at different pH and the isomerization rate was followed by HPLC analysis (Fig. S5). In all cases, after 2 min, the reactions have already reached the photo-stationary state consisting of an almost 1:1 mixture of both isomers. Once again, the isomerization occurs independently of the pH media, but observing, as before, a reduction of peptide signals on the HPLC traces due to their precipitation at neutral or basic conditions.

To confirm the stability of the system to the photoisomerization, the CP was subjected to several isomerization cycles (Fig. S6) and irradiated for long periods of time (60 min, Fig. S7), in both cases no other products were found. Moreover, no isomerization to the thermodynamically more stable *E*-isomer or decomposition was observed when a solution of **^{Z}CP1** was heated at 80 °C for 72 h (200 μM, Fig. S8). The above-mentioned signal reduction at neutral/basic conditions was also evaluated. For this purpose, the reaction mixtures were lyophilized and subsequently re-dissolved and analyzed by HPLC, confirming the recovery of both peptides (Fig. S9), but also the appearance of a new oxidized derivative in less than a 10%. This suggests that the aforementioned signals reduction is mainly due to precipitation and not to the decomposition of the cyclic peptides as a consequence of the irradiations. In fact, ultracentrifugation of the pH 7 reaction mixture after irradiation using the 254 nm wavelength showed the preferential accumulation of **^{E}CP1** (Fig. S10), the precursor of SCPNs, at the bottom of the sample, while the ratio of the other isomer is increased in the upper part of the sample. The accumulation of **^{E}CP1** at the bottom fraction suggests that self-assembly and nanotube formation must be the main reason of peptide precipitation.

Self-assembly properties and light-induced assembly/disassembly

The self-assembling properties (Fig. 2) of both peptides were evaluated, starting with their fluorescence properties. The spectra of **^{E}CP1** in double-distilled water (pH 3-5) showed the characteristic bands of monomeric pyrene moiety whose emission decreases upon basification (Fig. 2B). At pH 6, a new band around 475 nm, attributed to the pyrene excimer, started to raise.[25] Subsequent basification did not significantly change the ratio of monomer and excimer emission. Such behavior can be attributed to the stacking properties of the CP upon deprotonation of the imidazolium ring. At acidic pH, all the imidazole moieties are protonated, preventing the formation of the β-sheet structure because of the repulsion of cationic substituents. Upon neutralization,

the formation of hydrogen bonds between peptide backbones facilitates nanotube formation. In concentration-dependent experiments carried out at neutral pH, the band at 475 nm increased with rising CP concentration, confirming the supramolecular nature of excimer formation (Fig. S11A). Such behavior was not observed for the Z-isomer, whose emission properties did not change with the pH (Fig. S11B and S11C). Concentration-depending experiments in the presence of a β-sheet reporter were also carried out to further confirm that these differences resulted from the distinctive assembling properties of the CPs. To this end, Thioflavin T (ThT), a well-known dye that fluoresces upon binding to β-sheet structures, was selected.[26] The experiments were carried out at neutral conditions (10 mM HEPES pH 7.0, λ_{ex} = 440 nm). Addition of increasing amounts of **^{E}CP1** (1-200 μM) to a solution of ThT (20 μM) gave rise to an evident growth of dye emission that confirms the interaction of the dye with cyclic peptide assemblies (Fig. 2C). From these experiments we could estimate a critical aggregation concentration (*cac*) around 22 μM using the ThT emission at pH 7.0 (Fig. 2D). Similar *cac* was obtained at basic pH (9.0, Fig. S12); while at acidic pH (<4.5) the characteristic emission band of ThT did not change. This finding confirms the importance of imidazole protonation/deprotonation in the formation of SCPNs. Under neutral or basic conditions, SCPN formation should bring together the β-sheet reporter (ThT) and the pyrene moieties, consequently fluorescence resonance energy transfer (FRET) between both dyes (pyrene as a donor and ThT as acceptor) should confirm the spatial proximity between SCPNs and dye.[11] As expected, the FRET effect was only observed for experiments carried out in neutral-alkaline media, which indicated the relation of ThT emission with peptides assembled (Fig. S13). Similar experiments with the Z-isomer (**^{Z}CP1**) did not show significant changes in dye emission, confirming the incapability of this isomer to form β-sheet structures (Fig. S14).

To further understand the self-assembly properties of both peptides, circular dichroism (CD) studies were also performed to evaluate the different pH conditions for both isomers (Fig. 2E and S15). No CD signals corresponding to the pyrene moiety (353 nm) were detected at native pH (4.4) for both peptides at a similar concentration (350 μM), being this the only similarity between them. Basification of the solution of **^{Z}CP1** did not induce any change in its CD spectra (Fig. S15). On the contrary, as the pH increases for **^{E}CP1**, a strong CD signal was observed for the Pyr band,[12,27] showing a strong negative band at a pH higher than 5.7. Such an effect suggests chirality transfer from the peptide backbone to the pyrene unit with the formation of long-range-ordered supramolecular assemblies. These changes take place under similar conditions to the fluorescence studies, suggesting that the CD signal and ThT emission must be related to the CP assembly. Concentration-depending experiments showed the characteristic increase that confirms that the transfer of chirality must be related to the self-assembling process.

Once the spectroscopic fingerprints highlighting the different assembly properties in solution of both isomers of **CP1** were confirmed, electron microscopy studies were carried out to visualize the structural changes related to the supramolecular properties of these CPs. Scanning transmission electron microscopy (STEM) micrographs confirmed the presence of long linear structures, few μm long, that can be related to single or bundles of nanotubes of **^{E}CP1** (200 μM, Fig. 2F and S16) over a wide range of pH conditions (pH 5-9). This outcome confirms the ability of this isomer to stack forming nanotubes specially under neutral or slightly basic conditions. These self-assembly conditions, which resemble those of physiological media, offer a glimpse of possible applications for the development of new therapeutic tools. As expected, the length and thickness of these linear supramolecular structures are correlated with CP concentration; longer and thicker fibers were detected at higher concentrations. Nanotube dissociation can be accomplished by acidification (pH 2.0) without affecting peptide structure. The assembly and disassembly process can be induced by changing the pH for several cycles without affecting the peptide stability (Fig. S17). In contrast, none of the

solutions of **ᶻCP1** showed these types of structures; instead, amorphous aggregates were found (Fig. 2G and S18).
The SCPN diameter was assessed by AFM. Fig. 2H and S19 show the micrographs obtained after drop casting a 200 μM solution of **ᴱCP1** on mica. The images show the presence of polydisperse nanotubes in length that are randomly oriented on the mica surface. The height of individual nanotubes was on the order of 2.95 ± 0.32 nm, which corresponds to the expected for this type of SCPNs. As expected, no tubular structures were found for **ᶻCP1**.
Next, we employed Epifluorescence Microscopy to study the self-assembly process at the micrometer scale. Analysis of samples containing **ᴱCP1** (350 μM, 10 mM HEPES at pH 7.0, Fig. 2I) showed the hierarchical architecture preserved from the nanotubes to tens of micrometers long fibers. On the other hand, no clear fibrillar structures were observed in samples of **ᶻCP1** with emissions at shorter wavelengths all over the solution.
To determine whether light-induced isomerization is capable of triggering nanotube disassembly, we performed further irradiation studies on already assembled CPs at neutral pH (Fig. 3). For this purpose, a solution of **ᴱCP1** (200 μM) in HEPES (10 mM, pH 7.0) was irradiated at 254 nm and aliquots of reaction (400 μL) were taken every minute. These aliquots were mixed with a ThT (40 μM) solution under the same conditions (400 μL, 10 mM HEPES, pH 7.0), and the resulting samples (100 μM of **CP1** and 20 μM of ThT) were analyzed by fluorescence (Fig. 3D). At the initial conditions above the *cac* most of the **ᴱCP1** should be assembled forming SCPNs and, therefore, the interaction of ThT with the β-sheet structure of SCPN should give rise its characteristic emission. However, if amino acid isomerization induces CP folding, the ThT emission should change over time. Indeed, immediately after the first irradiation period, the characteristic band derived from the presence of the β-sheet structure starts to shrink. In addition, irradiated samples were taken every 2 min, deposited on carbon-coated grids and evaluated by STEM (Fig. 3E and S20A). Clearly, after 6 min, the STEM micrographs showed amorphous material together with few short persistence SCPNs. These outcomes confirm that isomerization of amino acid double bond can occur in the tubular structure, inducing SCPNs disassembly. Likewise, **ᶻCP1** isomerization under similar conditions (200 μM, HEPES 10 mM, pH 7.0) was also investigated (290-320 nm) and analyzed by fluorescence spectroscopy in a similar manner. In this case, the characteristic emission (494 nm) derived from CP planarization and nanotube formation was growing up (Fig. 3C). Moreover, nanotube formation after two minutes of irradiation was corroborated by STEM analysis (Fig. S20B). These experiments confirm that either assembly or disassembly of SCPNs can be triggered by light-induced isomerization of one single residue in a CP forming nanotubes. No restrictions on the olefin isomerization were found even if the CP is already assembled.

Assembling behavior in confined spaces

In the last years, microfluidic technology has become an effective method for analyzing molecular behavior, among other applications.[28,29] In general, microfluidics gives a more controlled environment than bulk, especially when aggregate visualization is required. Therefore, this technology allows for easy evaluation of the behavior of fibrillar and hydrogel-like supramolecular systems in confined spaces, especially for assessing their potential application as synthetic mimetics of cell cytoskeleton.[30]
Therefore, to further understand the process, we decided to evaluate the implications of externally induced isomerization to trigger the supramolecular polymerization in confined spaces using this technique.[11,12] Additionally, we could also evaluate the combination of the changes in pH or ionic strength with light input on the assembly process. We hypothesized that assembly changes could be monitored by following the different luminescence outputs of the pyrene monomer emission depending on the assembly state of the CPs. The microfluidic device shown in Fig. 4A was employed to control the tandem

assembly and droplet confinement of **CP1**. First, we induced peptide assembly in junction J_1 by merging the streams of I_{CP}, containing a slightly acidic solution of **CP1** (1.0 mM, pH ~3.0), and I_T, which contains a second solution responsible for inducing the corresponding changes in media conditions. These changes, such as neutralization or increase of ionic strength, should trigger the assembly process. Next, droplets formation was immediately achieved in the J_2 junction by flow focusing the aqueous stream with the oil stream (HFE 7500 3M Novec and 0.5 % v/v Pico-Surf as surfactant, I_{oil}).[31] This setup was employed to adjust the flow rates and the different stimuli.

Initial studies were carried out by merging the neutral buffered solution (20 mM HEPES pH 7.0, I_T) in J_1 with the aqueous solution of **^{Z}CP1** (1.0 mM, I_{CP}). As expected, the fluorescence microscopy analysis of the resulting droplets showed the typical self-quenched blue fluorescence emission characteristic of highly concentrated monomeric pyrene moieties that belongs to dispersed CPs (Fig. 4B). For the other isomer (**^{E}CP1**), the acidic aqueous solution (pH 3.0) also provided droplets with the typical quenched emission of monomeric species (Fig. S21). On the other hand, under neutral conditions, obtained by mixing the neutral buffered solution (20 mM HEPES, I_T) in J_1 with the aqueous solution of **^{E}CP1** (1.0 mM, I_{CP}), brighter blue-fluorescent droplets were obtained (Fig. 4C and S22) with fibril-*like* structures preferentially located in contact with the periphery of the droplets (Fig. S23). To our surprise, under these conditions the droplets had different sizes. Such behavior could be related with the presence of the SCPNs at the interface and not to the preparation method.[32]

Considering the possible fusion of vesicles induced by the nanotube at the micelle interface, we carried out additional experiments to further understand this process. Therefore, the formation and storing of the vesicles were followed at the microscope (Fig. 4D, video S1). Initially, all the droplets, after leaving the microfluidic tubing, had the same diameter. However, after resting for a few seconds, the fusion of neighboring vesicles starts to take place all over the media, confirming the fusiogenic properties dictated by the nanotubes.[33] To understand these fusion properties, droplets containing either of the two isomers of **CP1** were mixed to evaluate the invasive (parasitic) or self-invasive (narcissistic) properties of the resulting vesicles (Fig. 5A-C and S24). To follow the merging process, colored vesicles containing **^{Z}CP1** (1 mM, I_{CP}) were prepared by merging I_{CP} with an aqueous HEPES solution (20 mM, pH 7.0, I_T) containing 5-TAMRA (40 μM). Then, **^{E}CP1** droplets were collected over the **^{Z}CP1** droplets with 5-TAMRA in a 1:1 ratio. Droplets containing opposite isomers showed no tendency to fuse with each other, whereas vesicles that contain **^{E}CP1** maintained their self-fusiogenic properties. Therefore, it appears that this merging function requires the establishment of an intercommunication between the assembled nanotubes that are deposited at both interfaces of the neighboring droplets to dictate their fusion. To further understand the mechanism of nanotube-induced droplet fusion, a new peptide with an alkyl chain of six carbons (**^{E}CP4/ ^{Z}CP4**, Fig. 1) was prepared to evaluate the role of the pyrene moiety in this process. This peptide showed reduced self-assembly properties (Fig. S25) compared to **^{E}CP1**, forming nanotubes at higher concentrations, along with a lower propensity to form fibers as indicated by STEM images (Fig. S25C-D). Peptide **^{E}CP4** did not showed fusiogenic properties (Fig. S26), despite the microfluidic experiments were carried out at higher concentration (1.5 mM, I_{CP}). This suggest that the π,π-stacking of pyrene moieties not only plays a relevant role in the hierarchical formation of the supramolecular fibers, but also in eliciting droplet fusion. Most likely, under neutral conditions, nanotube assembly in the droplet might induce the formation of a hydrophobic surface that would interact with the droplet interface, exposing the pyrene moieties exposed towards the oil media. The contact of two neighboring droplets interfaces might induce, in the case of **^{E}CP1**, the aggregation of the pyrene moieties, guided by the π,π-stacking,[11,12,18] resulting in vesicle fusion (Fig. 5E).

The SCPNs formation was also evaluated by increasing the ionic strength of the media (Fig. S27).[11] Therefore, a $CaCl_2$ (1.0 M, I_T) solution was merged in J_1 with

the acidic solution of **^{E}CP1** on I_{CP}. Under these conditions, vesicles with fiber-*like* structures were also observed, confirming that self-assembly can also be triggered by modulation of the ionic strength of the media (Fig. S28). In this case, the supramolecular fibers seem to be distributed throughout the water droplet internal volume, as already reported with a different peptide,[11] and the resulting droplets presented reduced fusiogenic properties, most likely due to the different properties of the resulting nanotubes.

Finally, the light-induced assembly on the droplet was also assessed. To this end, vesicles containing **^{Z}CP1** (1.0 mM, I_{CP}) were prepared by merging I_{CP} with the HEPES solution (20 mM, pH 7.0, I_T) at J_1. The resulting droplets were stored and analyzed by fluorescence microscopy. The vesicles showed the typical quenched blue fluorescence emission previously mentioned. These vesicles were irradiated using a 290-320 nm lamp for 5 min (Fig. 5D and S29). After 2 min, clear emissions with fibrillar shape structures were observed at the droplet, confirming the isomerization-triggered assembly of the CP in the confined environment. The resulting vesicles were lysed by adding a TFA aqueous solution (0.1% v/v) and sonicated for 30 sec. The supernatant of the resulting aqueous solution was analyzed by HPLC showing similar photostationary state with a 7:3 ratio between **^{E}CP1**:**^{Z}CP1** as found in solution.

CONCLUSIONS

We have shown how the ability to precisely control a switchable structure enables the robust design of novel tubular-shaped photo-assemblers. For this purpose, we have designed a new cyclic peptide containing an unsaturated ß-amino acid, whose irradiation with the appropriate wavelength allowed the isomerization of the aforementioned residue between the *Z*- and the *E*-forms. While the *cis*-isomer adopts a folded conformation driven by the strong intramolecular hydrogen bonding of the unsaturated residue that constrains its assembly properties, the *trans*-isomer adopts a planar conformation that facilitate the stacking and the formation of a tubular-shaped supramolecular polymer. Such assembly process occurs only at appropriate pH (5.6-9.5) due to the selective protonation/deprotonation of basic residues, allowing a dual checkpoint control over nanotube formation. The isomerization and the different properties of both isomers were proven by different techniques, such as NMR, fluorescence/CD spectroscopy, STEM or AFM. Finally, the spatial controlled polymerization of cyclic peptides to form microfibrillar bundles in confined aqueous droplets was addressed by a microfluidic regulated tandem process. This method not only allowed the visualization of supramolecular polymerization triggered by light and media, but also the precise preferential localization of fibers at the periphery or into the core of the droplets. The nanotubes generated under neutral conditions, those formed at the interface, exhibit fusiogenic properties inducing droplets merging. Nanotube formation only takes place under appropriate environmental conditions for the *E*-isomer cyclic peptide. This work fully demonstrates the control over the supramolecular polymerization of synthetic fibers in artificial minimal models. The fusiogenic properties of this photoassemblers might find applications in the development of novel delivery systems of therapeutic agents, such as proteins (antibodies or enzymes), for the treatment of various diseases. These systems should contain the non-stackable form of the CP at the vesicle interface to form the nanotubes upon light irradiation and trigger the vesicles fusion with target cells.

EXPERIMENTAL PROCEDURES

Resource availability

Lead contact

Further information and requests for resources should be directed to and will be fulfilled by the lead contact, Juan R. Granja (juanr.granja@usc.es).

Materials availability
All materials generated in this study are available from the lead contact on request.

Data and code availability
The published article includes all datasets generated or analyzed during this study.

SUPPLEMENTAL INFORMATION

Supplemental information can be found online at https://doi.org/. Supplemental figures (Fig. S30-S45) can be found at the synthesis and characterization section.

ACKNOWLEDGMENTS

This work was supported by the Spanish Agencia Estatal de Investigación (AEI) and the ERDF (PID2019-111126RB-100), and by the Xunta de Galicia and the ERDF (ED431C 2021/21 and Centro singular de Investigación de Galicia accreditation 2019–2022, ED431G 2019/03). We also thank the ORFEO-CINCA network and Mineco (RED2018-102331-T). M.V. thanks the Spanish Ministry of Universities for his FPU contract.

AUTHOR CONTRIBUTIONS

M.V. and F.N. designed and synthesized the molecular structures, carried out the experimental work and analyzed the data; G.M. synthetize the unsaturated amino acid; A.P. helped in the synthesis of CP; A.M.-A. helped in the microfluidic experiments; M.A., A.M., F.N. and J.R.G. devised the project. M.V., F.N. and J.R.G. wrote the manuscript.

DECLARATION OF INTERESTS

The authors declare no competing interests.

REFERENCES*

1. Zhang, Q., Qu, D. and Tian, H. (2019). Photo-Regulated Supramolecular Polymers: Shining Beyond Disassembly and Reassembly. Adv. Opt. Mater. *7*, 1900033. *10.1002/adom.201900033*
2. Chen, J., Leung, F.K.-C., Stuart, M.C.A., Kajitani, T., Fukushima, T., van der Giessen, E., Feringa, B.L. (2017). Artificial muscle-like function from hierarchical supramolecular assembly of photoresponsive molecular motors. Nat. Chem. *10*, 132–138. 10.1038/nchem.2887.
3. Jerca, F.A., Jerca, V.V. and Hoogenboom, R. (2022). Advances and opportunities in the exciting world of azobenzenes. Nat. Rev. Chem. *6*, 51–69. 10.1038/s41570-021-00334-w.
4. Albert, L., Vázquez, O. (2019). Photoswitchable peptides for spatiotemporal control of biological functions. Chem. Commun. *55*, 10192–10213. 10.1039/C9CC03346G.
5. Gutiérrez-Salazar, M., Santamaría-Aranda, E., Schaar, L., Salgado, J., Sampedro, D., Lorenz-Fonfria, V.A. (2019). A photoswitchable helical peptide with light-controllable interface/transmembrane topology in lipidic membranes. IScience *24*, 102771. 10.1016/j.isci.2021.102771.
6. Marafon, G., Crisma, M., Moretto, A. (2019). Tunable E-Z photoisomerization in α,β-peptide foldamers featuring multiple (E/Z)-3-aminoprop-2-enoic acid units. Org. Lett. *21*, 4182–4186. 10.1021/acs.orglett.9b01360.
7. Marafon, G., Crisma, M., Moretto, A. (2018). Intrinsically Photoswitchable α/ß Peptides toward Two-State Foldamers. Angew. Chem. Int. Ed. *57*, 10217–10220. 10.1002/anie.201806035.
8. Marafon, G., Crisma, M., Masato, A., Plotegher, N., Bubacco, L., Moretto, A. (2021). Photoresponsive Prion-Mimic Foldamer to Induce Controlled Protein Aggregation. Angew. Chem. Int. Ed. *60*, 5173–5178. 10.1002/anie.202012995.
9. Song, Q., Cheng, Z., Kariuki, M., Hall, S.C.L., Hill, S.K., Rho, J.Y., Perrier, S. (2021). Molecular Self-Assembly and Supramolecular Chemistry of Cyclic Peptides. Chem. Rev. *121*, 13936–13995. 10.1021/acs.chemrev.0c01291.
10. Rodríguez-Vázquez, N., Amorín, M., Granja, J.R. (2017). Recent advances in controlling the internal and external properties of self-assembling cyclic peptide nanotubes and dimers. Org. Biomol. Chem. *15*, 4490–4505. 10.1039/c70b00351j.

11. Méndez-Ardoy, A., Bayón-Fernández, A., Yu, Z., Abell, C., Granja, J.R., Montenegro, J. (2020). Spatially Controlled Supramolecular Polymerization of Peptide Nanotubes by Microfluidics. Angew. Chem. Int. Ed. *59*, 6902–6908. 10.1002/anie.202000103.

12. Méndez-Ardoy, A., Granja, J.R., Montenegro, J. (2018). pH-Triggered self-assembly and hydrogelation of cyclic peptide nanotubes confined in water micro-droplets. Nanoscale Horiz. *3*, 391–396. 10.1039/c8nh00009c.

13. Song, Q., Goia, S., Yang, J., Hall, S.C.L., Staniforth, M., Stavros, V.G., Perrier, S. (2021). Efficient Artificial Light-Harvesting System Based on Supramolecular Peptide Nanotubes in Water. J. Am. Chem. Soc. *143*, 382–389. 10.1021/jacs.0c11060.

14. Song, Q., Yang, J., Rho, J. Y., Perrier, S. (2019). Supramolecular switching of the self-assembly of cyclic peptide–polymer conjugates via host–guest chemistry. *Chem. Commun. 55*, 5291–5294. 10.1039/c9cc01914f.

15. Yang, J., Song, J.-I., Song, Q., Rho, J.Y., Mansfield, E.D.H., Hall, S.C.L., Sambrook, M., Huang, F., Perrier, S. (2020). Hierarchical Self-Assembled Photo-Responsive Tubisomes from a Cyclic Peptide-Bridged Amphiphilic Block Copolymer. Angew. Chem. Int. Ed. *59*, 8860–8863. 10.1002/anie.201916111.

16. Cissé, N., Kudernac, T. (2020). Light-Fuelled Self-Assembly of Cyclic Peptides into Supramolecular Tubules. ChemSystemsChem *2*, e2000012. 10.1002/syst.202000012.

17. Chernomordik, L. (1996). Non-bilayer lipids and biological fusion intermediates. Chem. Phys. Lipids *81*, 203–213. 10.1016/0009-3084(96)02583-2.

18. Novelli, F., Vilela, M., Pazó, A., Amorín, M., Granja, J.R. (2021) Molecular Plumbing to Bend Self-Assembling Peptide Nanotubes. Angew. Chem. Int. Ed. *60*, 18838–18844. 10.1002/anie.202107034.

19. Ghadiri, M.R., Granja, J.R., Milligan, R.A., McRee, D.E., Khazanovich, N. (1993). Self-Assembling Organic Nanotubes Based on a Novel and Rational Designed Peptide Architecture. Nature *366*, 324–327. 10.1038/366324a0.

20. Silk, M.R., Newman, J., Ratcliffe, J.C., White, J.F., Caradoc-Davies, T., Price, J.R., Perrier, S., Thompson, P.E., Chalmers, D.K., (2017). Parallel and antiparallel cyclic D/L peptide nanotubes. Chem. Commun. *53*, 6613–6616. 10.1039/c7cc00846e.

21. Clark, T. D., Buriak, J.M., Kobayashi, K., Isler, M.P., McRee, D.E., Ghadiri, M.R. (1998). Cylindrical β-Sheet Peptide Assemblies. J. Am. Chem. Soc. *120*, 8949–8962. 10.1021/ja981485i.

22. Rovero, P., Quartara, L., Fabbri, G. (1991). Synthesis of cyclic peptides on solid support. Tet. Lett. *32*, 2639–2642. 10.1016/S0040-4039(00)78806-X.

23. González-Freire, E., Novelli, F., Pérez-Estévez, A., Seoane, R., Amorín, M., Granja, J.R. (2021). Double orthogonal click reactions for the development of antimicrobial peptide nanotubes. Chem. Eur. J. *27*, 3029–3038. 10.1002/chem.202004127.

24. Krimm, S. Bandekar, J. (1986). Vibrational spectroscopy and conformation of peptides, polypeptides, and proteins. In Advances in Protein Chemistry, C.B. Anfinsen, J.T. Edsall, F.M. Richards, eds. (Academic Press) vol. 38, pp. 181–364. 10.1016/s0065-3233(08)60528-8.

25. J. Montenegro, J., Vázquez-Vázquez, C., Kalinin, A., Geckeler, K.E., Granja, J.R. (2014). Coupling of carbon and peptide nanotubes. J. Am. Chem. Soc. *136*, 2484–2491. 10.1021/ja410901r.

26. Groenning, M.J. (2010). Binding mode of Thioflavin T and other molecular probes in the context of amyloid fibrils—current status. Chem. Biol. *3*, 1–18. 10.1007/s12154-009-0027-5.

27. Nishikawa, T., Tajima, N., Kitamatsu, M., Fujiki, M., Imai, Y. (2015). Circularly polarised luminescence and circular dichroism of L- and D-oligopeptides with multiple pyrenes. Org. Biomol. Chem., *13*, 11426–11431. 10.1039/C5OB01710F.

28. Whitesides, G.M. (2006). The origins and the future of microfluidics. Nature *442*, 368–373. 10.1038/nature05058.

29. Shang, L., Cheng, Y., Zhao, Y. (2017). Emerging Droplet Microfluidics. Chem. Rev. *117*, 7964–8040. 10.1021/acs.chemrev.6b00848.

30. Zhan, P., Jahnke, K., Liu. N., Göpfrich, K. (2022). Functional DNA-based cytoskeletons for synthetic cells. Nat. Chem. *14*, 958-963. 10.1038/s41557-022-00945-w.

31. C. Holtze, C., Rowat, A.C., Agresti, J.J., Hutchison, J.B., Angil, F.E., Schmitz, C.H.J., Kster, S., Duan, H., Humphry, K.J., Scanga, R.A., Johnson, J.S., Pisignano, D., Weitz, D.A. (2008). Biocompatible surfactants for water-in-fluorocarbon emulsions. Lab Chip *8*, 1632–1639. 10.1039/B806706F.

32. Epand, R. M. (2003). Fusion peptides and the mechanism of viral fusion. Biochim. Biophys. Acta *1614*, 116–121. 10.1016/S0005-2736(03)00169-X.

33. Theberge, A.B., Courtois, F., Schaerli, Y., Fischlechner, M., Abell, C., Hollfelder, F., Huck W.T.S. (2010). Microdroplets in Microfluidics: An Evolving Platform. Angew. Chem. Int. Ed. *49*, 5846–5868. 10.1002/anie.200906653.

FIGURES AND LEGENDS

Figure 1. Synthetic scheme and isomerization studies.

(A) Illustration of the synthetic scheme used for the preparation of CPs (**CP2/CP3**, **^{Z}CP1**/**^{E}CP1** and **^{Z}CP4**/**^{E}CP4**).
(B) Pilled chromatograms corresponding to the kinetic study at pH 5.1 of the isomerization of **^{Z}CP1** into **^{E}CP1** (200 μM) by irradiation with 290-320 nm wavelength. An aqueous solution of 4-aminobenzoic acid (ABA, 0.01 mg/mL) was added as an internal standard to quantify the peptide concentration.
(C) Time-dependent conversion of **^{Z}CP1** into **^{E}CP1.**
(D) Pilled chromatograms corresponding to the kinetic study at pH 4.6 of the isomerization of **^{E}CP1** into **^{Z}CP1** (200 μM) by irradiation with 254 nm wavelength. An aqueous solution of 4-aminobenzoic acid (ABA, 0.01 mg/mL) was added as an internal standard to quantify the peptide concentration.
(E) Time-dependent conversion of **^{E}CP1** into **^{Z}CP1.**

Figure 2. Characterization and nanotube forming properties of ^{E}CP1.

(A) Model proposed for the self-assembly process. The amino acid side chains in the nanotube model are omitted for clarity.
(B) Fluorescence emission of **^{E}CP1** (100 μM) in water (λex = 340 nm) at different pH by adjusting the media by addition of small aliquots of NaOH (0.1 M).
(C) Overlaid ThT (20 μM) fluorescence spectra of solutions of **^{E}CP1** in HEPES (10 mM, pH 7.0) at different concentrations (λex = 440 nm).
(D) Intensity ratio I_{494}/I_0 versus the concentration of **^{E}CP1**. I_0 is the fluorescence intensity at 494 nm of ThT alone. Spectra were recorded at 20°C. The break point indicates a *cac* of 22 μM.
(E) CD spectra of **^{E}CP1** (350 μM) in water at different pH. The pH was adjusted by adding NaOH (0.1M).
(F) STEM micrograph achieved by deposition from a solution of **^{E}CP1** (200 μM, 10 mM HEPES at pH 7.0) on Cu grids. Staining was obtained with 2 % w/v phosphotungstic acid (PTA). Scale bar 200 nm.
(G) STEM micrograph achieved by deposition from a solution of **^{Z}CP1** (200 μM, 10 mM HEPES at pH 7.0) on Cu grids. Staining was obtained with 2 % w/v phosphotungstic acid (PTA). Scale bar 200 nm.
(H) AFM micrograph of **^{E}CP1** (200 μM, 10 mM HEPES at pH 7.0) on mica. The height profiles (right) were achieved along the color lines (red, green and blue) shown in the image.
(I) Representative epifluorescence image of SCPNs deposited on a standard glass microscopy slide from a solution of **^{E}CP1** (350 μM) in HEPES (10 mM, pH 7.0). Scale bar: 20 μm.

Figure 3. Studies of light induced nanotube assembly/disassembly by CP interconversion (^{E}CP1 ⇄ ^{Z}CP1) at different conditions.

(A) Illustration of the photo-modulated assembly/disassembly process of peptide nanotubes at different pH. The amino acid side chains in the nanotube model are omitted for clarity.
(B) HPLC analysis of the irradiation (290-320 nm) of an aqueous solution of **^{Z}CP1** (200 μM) at pH 7.0 (HEPES, 10 mM) after different time intervals. After 2 minutes of irradiation (purple line), the formation of a new product (**^{E}CP1**) is distinctly observable.
(C) Fluorescence analysis (overlaid of ThT (20 μM) fluorescence emission band) of **^{Z}CP1** (100 μM) irradiated with a 290-320 nm wavelength lamp at pH 7.0 (HEPES, 10 mM). 400 μL aliquots of CP at 200 μM were taken every minute, mixed with a 40 μM ThT solution (400 μL in 10 mM HEPES, pH 7.0) and then analyzed in the fluorimeter.
(D) Fluorescence analysis (overlaid of ThT (20 μM) fluorescence emission band) of nanotube dissociation by irradiation a solution of **^{E}CP1** (100 μM) with a 254 nm wavelength lamp at pH 7.0 (HEPES, 10 mM). 400 μL aliquots of CP at 200 μM were taken every minute, mixed with a 40 μM ThT solution (400 μL in 10 mM HEPES, pH 7.0) and then analyzed in the fluorimeter.
(E) STEM micrographs achieved by deposition on Cu grids at different reaction time of solutions of **^{E}CP1** (25 μM) irradiated with a 254 nm wavelength lamp at pH 7.0 (HEPES, 10 mM). Staining was obtained with 2 % w/v phosphotungstic acid (PTA). STEM micrographs were acquired at an extra high tension of 20kV.

Figure 4. Stimuli mediated self-assembly of ^{E}CP1 in microfluidic generated droplets.

(A) Microfluidic device for the *in-situ* nanotube formation. Channels dimensions: 35 x 50 μm. CPs (^{Z}**CP1** or ^{E}**CP1**) in aqueous media (1.0 mM, milliQ water, pH 2–3) were injected in inlet I_{CP} (blue) at flow rate of 300 μL h^{-1} and assembled upon mixing at J_1 with inlets I_T (red) containing aqueous HEPES (20 mM, pH 7.0) or $CaCl_2$ (1.0 M) at flow rate of 150 μL h^{-1}. The aqueous stream converges in J_2 with the oil phase at inlet I_{oil} (HFE 7500 3M Novec with 0.5 % v/v Pico-Surf as surfactant, black) at flow rate of 500 mL h^{-1} for droplet generation. Droplets are collected in the outlet. In the figure, the collection of B or C droplets corresponds to independent experiments.
(B) Microfluidic droplets (water-in-oil) of ^{Z}**CP1** at pH 7.0. I_{CP} is an aqueous solution of ^{Z}**CP1** (1.0 mM) and I_T is HEPES (20 mM, pH 7.0). Scale bar: 100 μm.
(C) Self-assembly of ^{E}**CP1** into microfluidic-generated droplets (water-in-oil). An aqueous solution of ^{E}**CP1** (1.0 mM) at I_{CP} is mixed with the buffered HEPES solution (20 mM, pH 7.0, I_T) at J_1. Scale bar: 100 μm.
(D) Microscope images at different times (0, 12, 24 and 36 s) of droplets prepared at neutral pH, showing the vesicles fusiogenic properties induced by SCPNs generated at the interface. Scale bar: 100 μm.

Figure 5. Studies of fusiogenic properties of droplets induced by cyclic peptide nanotubes.

(A) Brightfield, (B) epifluorescence pyrene emission and (C) epifluorescence 5-TAMRA emission images of ^{E}**CP1** droplets mixed with ^{Z}**CP1** droplets with 5-TAMRA in a 1:1 ratio. (D) Microfluidic droplets (water-in-oil) of ^{Z}**CP1** at pH 7.0 after 5 min irradiation with a 290-320 nm lamp in which bright fiber-*like* structures are observed. (E) Proposed model of droplet fusion based on the hierarchical process of SCPNs at the interfaces.

Figure1

Click here to access/download;Figure;Fig.1(CHEMJOURNAL-D-23-00714R1).tiff

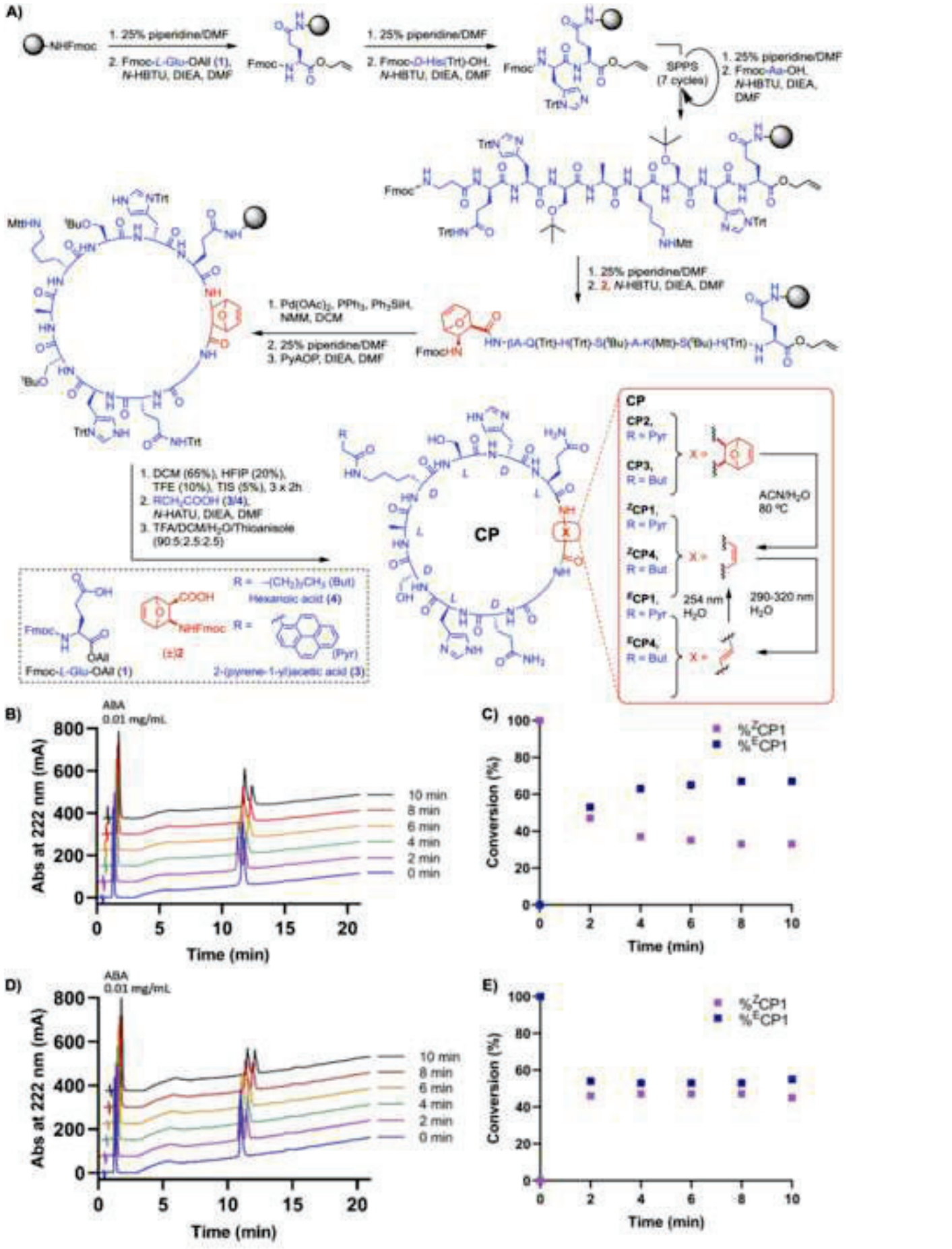

Figure2

Click here to access/download;Figure;Fig.2(CHEMJOURNAL-D-23-00714R1).tiff

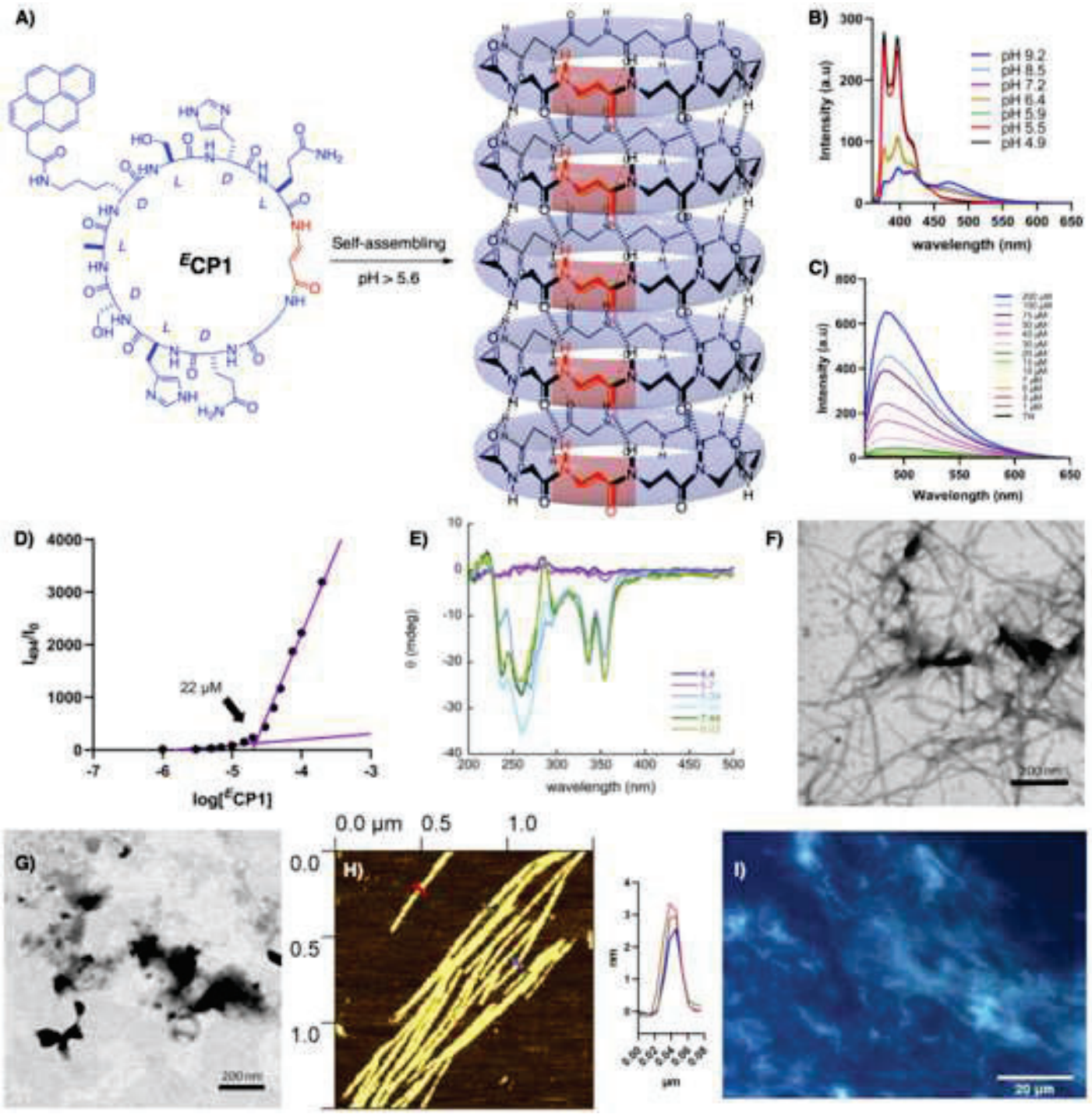

Click here to access/download;Figure;Fig.3(CHEMJOURNAL-D-23-00714R1).tiff

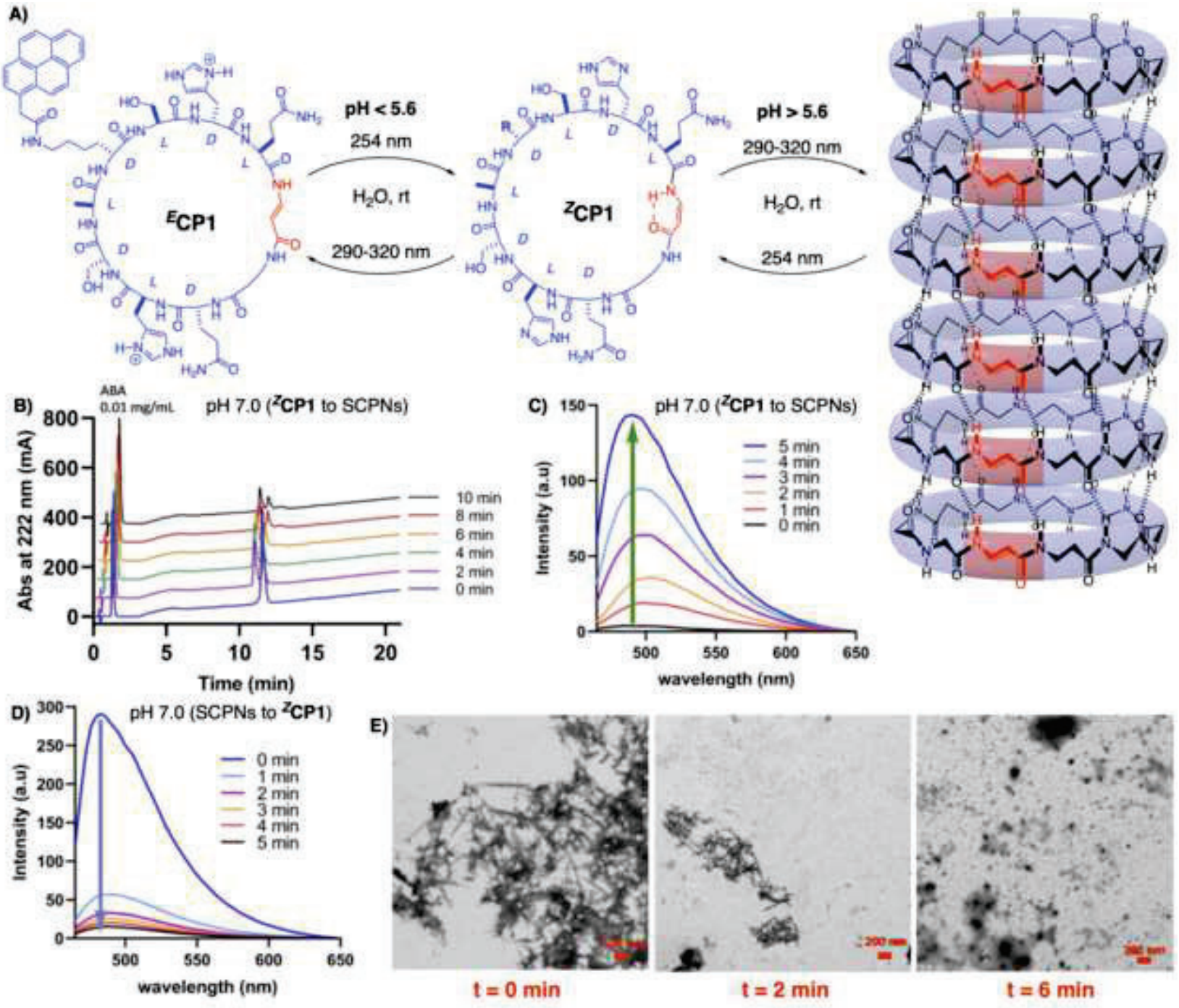

Figure4

Click here to access/download;Figure;Fig.4(CHEMJOURNAL-D-23-00714R1).tiff

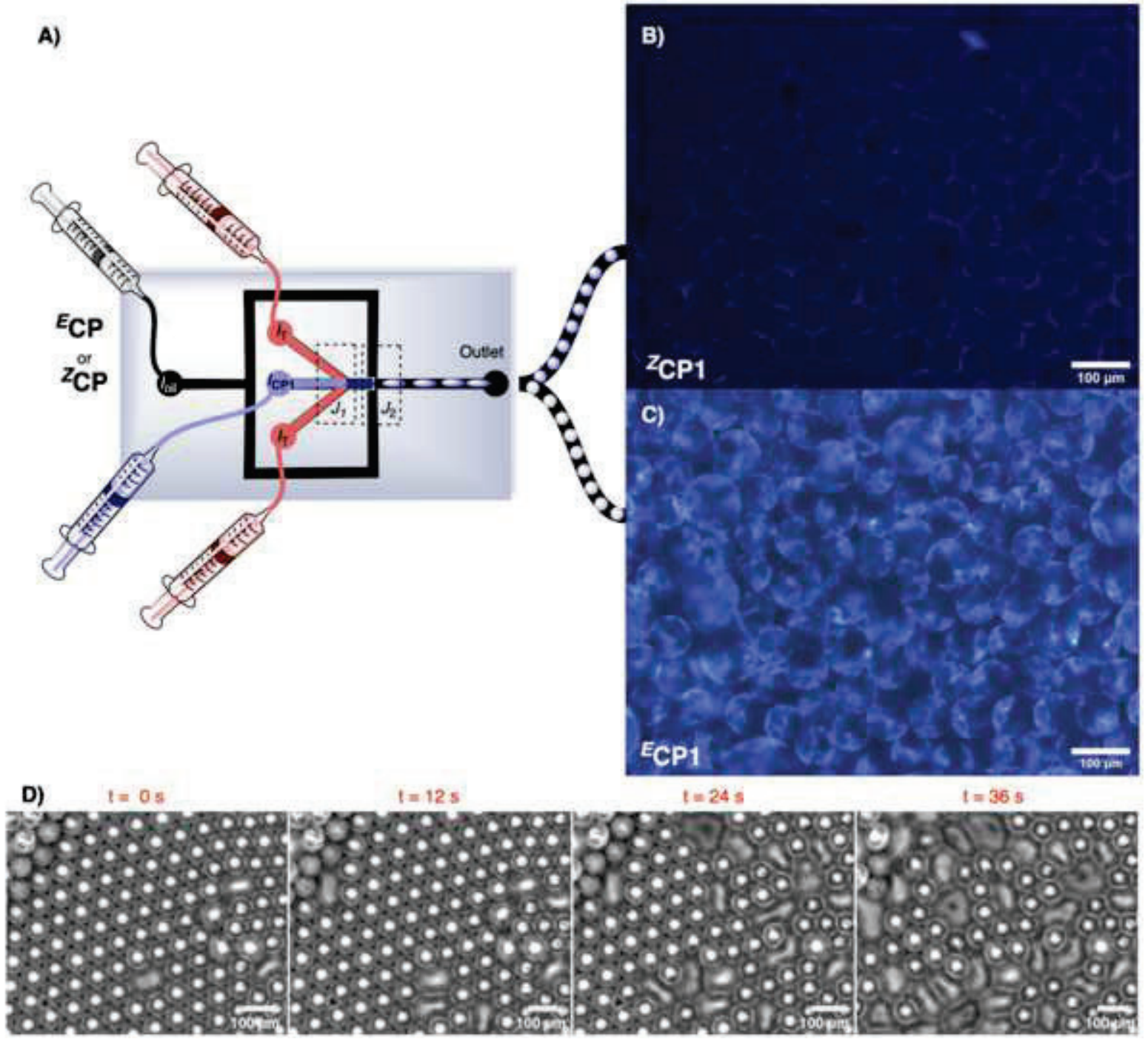

Figure5

Click here to access/download;Figure;Fig.5(CHEMJOURNAL-D-23-00714R1).tiff

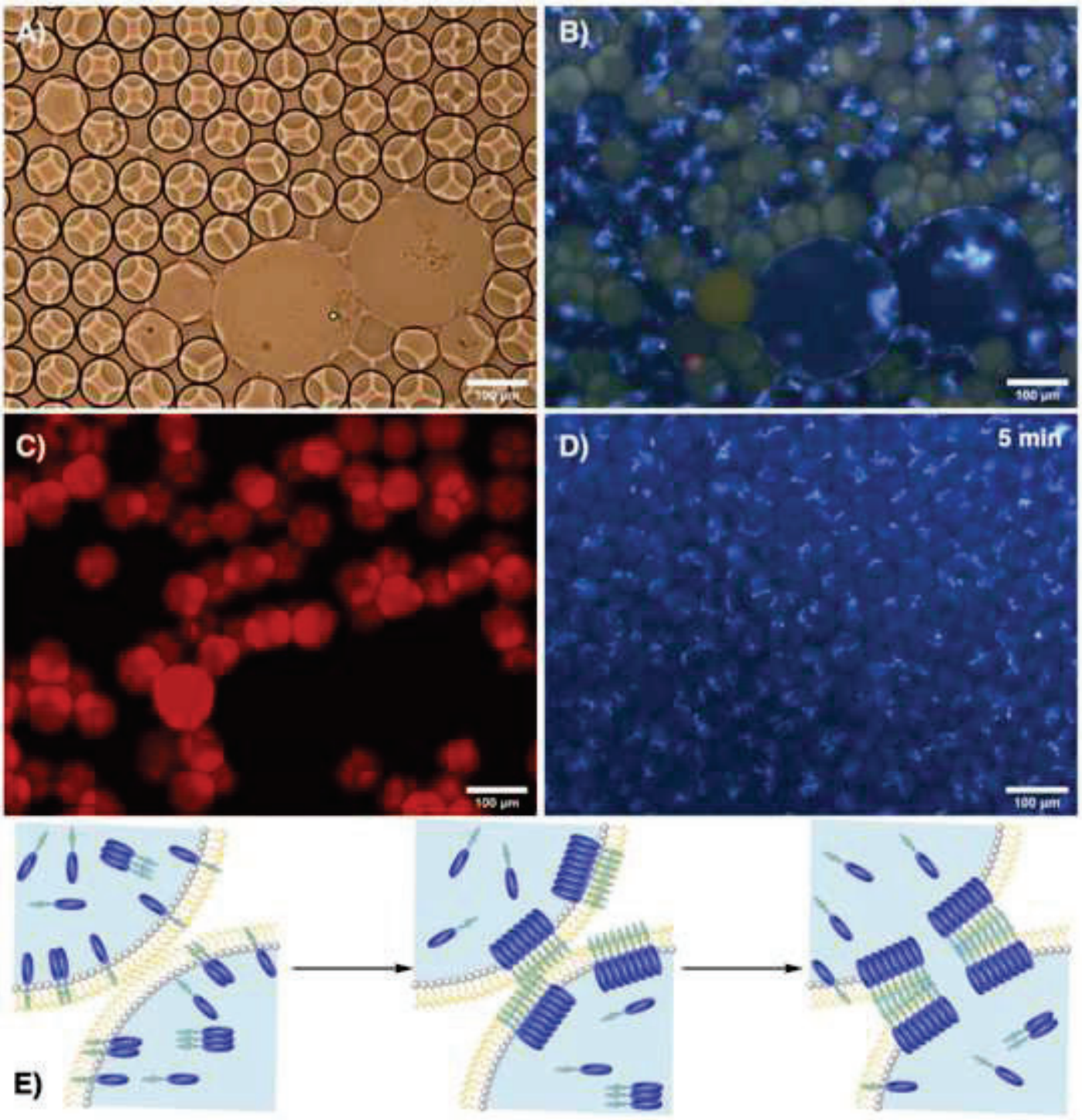

CoverArt(proposal)

Click here to access/download;Figure;Cover(CHEMJOURNAL-D-23-00714R1).tif